Solution Structure and Phosphopeptide Binding to the N-terminal Domain of *Yersinia* YopH: Comparison with a Crystal Structure†

Purnima Khandelwal,‡,§ Kai Keliikuli,‡ Craig L. Smith,‡,|| Mark A. Saper,‡,⊥ and Erik R. P. Zuiderweg*,‡,⊥,#

Biophysics Research Division and Departments of Biological Chemistry and Chemistry, University of Michigan, 930 North University Avenue, Ann Arbor, Michigan 48109-1055

Received June 20, 2002; Revised Manuscript Received July 31, 2002

ABSTRACT: Virulence of pathogenic bacteria of the genus *Yersinia* requires the injection of six effector proteins into the cytoplasm of host cells. The amino-terminal domain of one of these effectors, the tyrosine phosphatase YopH, is essential for translocation of YopH, as well as for targeting it to phosphotyrosine-containing substrates of the type pYxxP. We report the high-resolution solution structure of the N-terminal domain (residues 1−129) from the *Yersinia pseudotuberculosis* YopH (YopH-NT) in complex with *N*-acetyl-DEpYDDPF-NH_2, a peptide derived from an in vivo protein substrate. In contrast to the domain-swapped dimer observed in a crystal structure of the same protein (Smith, C. L., Khandelwal, P., Keliikuli, K., Zuiderweg, E. R. P., and Saper, M. A. (2001) *Mol. Microbiol. 42*, 967−979), YopH-NT is monomeric in solution. The peptide binding site is located on a β-hairpin that becomes the crossover point in the dimer structure. The binding site has several characteristics that are reminiscent of SH2 domains, which also bind to pYxxP sequences.

The bacterium *Yersinia pseudotuberculosis* causes a range of gastrointestinal diseases in humans and rodents. The virulence of all *Yersinia* pathogenic species requires injection of at least six effectors proteins into host cells by a type III secretion system (*1*). One of these, YopH (***Y****ersinia* **o**uter **p**rotein **H**) is a 51-kDa effector protein that helps block phagocytosis in host macrophages, thus allowing the bacteria to evade the host immune response (*2*). YopH is a two-domain protein with three discernible functions. At the carboxyl end is a tyrosine phosphatase catalytic domain (residues 190−468) that is structurally similar to homologous eukaryotic enzymes (*3*, *4*). In the host cell, this domain selectively dephosphorylates proteins associated with focal adhesions, thus disrupting host signaling pathways (*5*, *6*). The amino-terminal 129 residues comprise a domain with the two other functions. The first 70 residues bind to the bacterial chaperone protein SycH (*7*) and are essential for secretion and translocation. The same YopH N-terminal domain also binds phosphotyrosine-containing protein sequences of the type pYXXP that target it and the catalytic domain to substrates in the infected host cell (*8*).

At least two host cell proteins, $p130^{Cas}$ and SKAP-HOM, were shown to be cellular substrates of the YopH catalytic domain (*2*, *9*). $p130^{Cas}$ is a scaffold protein that coordinates tyrosine-kinase-based signaling related to cell adhesion and induction of cell migration. It has 15 presumed tyrosine phosphorylation sites that contain the known YopH substrate motif DEpYXXP and are dephosphorylated following infection. It was shown that binding of residues 1−129 of YopH (YopH-NT) to $p130^{Cas}$ in a phosphotyrosine-dependent manner was necessary for efficient dephosphorylation (*8*). SKAP-HOM is a Src-associated adaptor protein which becomes phosphorylated following T cell activation (*10*). It was suggested that dephosphorylation of SKAP-HOM by YopH (also at a pYXXP site) allows *Yersinia* to interfere with the adhesion-regulated signal transduction pathway in macrophages (*2*).

The specificity of YopH-NT binding is similar to SH2 domains (including Crk which can bind and phosphorylate $p130^{Cas}$) that recognize pYXX(X)P protein sequences and are important in many signal transduction pathways (*11*, *12*). However, no significant amino acid homology exists between these functionally similar proteins (*13*).

Study of the structure and function of YopH-NT is not only of interest for the understanding of the pathogenic action of YopH itself, but also for insight into the mechanism of pathogenesis for other bacteria which encode type III secretion systems. Furthermore, discovering details of how phosphopeptides bind to YopH-NT and solving the structure of the complex are important for the understanding of the biochemical mechanism of YopH. It is possible that other effectors may utilize noncatalytic domains for substrate localization. Elucidation of its structure and function might contribute to development of antibacterial agents designed to render bacteria avirulent by inhibiting the proteins injected by the type III secretion system, rather than killing the bacteria.

† E.R.P.Z. was supported by Grants GM-52406 and GM-52421 and M.A.S. by Grant AI-34095. The Keck Foundation, NIH, and NSF are acknowledged for support of the 800 MHz system.

* To whom correspondence should be addressed. Phone: (734) 936-3850. Fax: (734) 764-3323. E-mail: zuiderwe@umich.edu.

‡ Biophysics Research Division.

§ Present address: Discovery Analytical Chemistry, Wyeth Research, CN 8000, Princeton, NJ 08543-8000.

|| Present address: Dept. of Molecular Microbiology, Washington Univ. School of Medicine, 660 South Euclid Avenue, St Louis, MO 63110-1093.

⊥ Department of Biological Chemistry.

Department of Chemistry.

10.1021/bi026333l CCC: $22.00
Published on Web 08/30/2002

Recently, two groups have reported crystal structures for similar constructs of the YopH-NT protein fragment. Despite apparently similar crystals, one group interpreted the data as a monomeric structure (*14*), whereas the other group reported a domain-swapped dimer where residues 1−29 crossover and fold with another YopH-NT molecule (*13*). Other than the crossover residue, both structures are identical. Neither group has succeeded in cocrystallizing the protein with a substrate peptide or protein. To help resolve the question whether YopH-NT is monomeric or dimeric in solution, we report the solution structure determination of the same construct using multidimensional multinuclear nuclear magnetic resonance (NMR)[1] methods. We establish that YopH-NT is monomeric in solution under the experimental conditions and that its high-resolution structural model, based on over 3200 experimental restraints, is similar to the model derived from the X-ray data as reported by Evdokimov et al. (*14*).

We determined the solution structure for YopH-NT in complex with the peptide Ac-DEpYDDPF-NH_2 derived from the murine host protein target SKAP-HOM. We have been able to obtain several intermolecular NOEs that delineate the location of the phosphopeptide on the protein surface. The binding surface of YopH-NT has several characteristics that are reminiscent of the binding surface of Crk SH2 domains. However, the binding pockets appear shallower. No significant long-range conformational changes take place in YopH upon binding of the peptide. Our studies indicate that the peptide-binding site in the apo form is inherently dynamic at the milli/microsecond time scale. The dynamics is not quenched upon substrate binding. By comparing the results of NMR titrations with two different phosphopeptides, we estimate an equilibrium dissociation constant of 1×10^{-7} M for Ac-DEpYDDPF-NH_2. We also estimate that about 70% of the binding free energy is associated with the pY interaction.

MATERIALS AND METHODS

Sample Preparation. The NMR samples of *Y. pseudotuberculosis* YopH-(1−129)-Ser-His_6 (YopH-NT) protein and its complex with Ac-DEpYDDPF-NH_2 were in 50 mM Na phosphate pH 6.5, 0.05% NaN_3, 5% ^2H_2O in water. The final concentration of the protein was ~0.8 mM, and the molar ratio of peptide to protein was 1.2:1. In addition, a fractionally ^{13}C-labeled sample for the stereospecific assignments of Leu and Val was prepared following the method described in ref *15*. The titrations with Ac-DEpYDDPF-NH_2 and the phosphotyrosine peptide DADEpYL (derived from epidermal growth factor receptor) were analyzed with a ^{15}N-^1H HSQC experiment by adding concentrated peptide in the same buffer and pH as the protein solution. Absolute concentrations of the protein solutions were indirectly estimated using a Bradford assay; relative concentrations of proteins and peptides were determined directly by 1D ^1H NMR spectroscopy.

NMR Spectroscopy and Resonance Assignments. NMR spectra were recorded on Varian 800 MHz Inova or Bruker Avance 500 MHz spectrometers, at 25 °C. All data were processed using NMRPipe (*16*) and analyzed with XEASY (*17*). Relaxation data was analyzed using NMRView (*18*). Sequential assignments were carried out independently for the apo-protein and the complex with Ac-DEpYDDPF-NH_2, as described by (*19*). Further NMR experiments that provided data for structure calculations were performed only on the complex. Stereospecific assignments were obtained for 26 out of 31 Leu and Val residues. 3D ^{15}N (80 ms), ^{13}C (120 ms), $^{15}N^{13}C$ (100 ms), and $^{13}C^{13}C$ (120 ms) resolved ^1H-^1H NOESY spectra were all recorded using the same sample in H_2O and were assigned to obtain distance restraints for structure calculations. The ^{13}C-edited experiments were folded once in the ^{13}C dimension with spectral width of 6000 Hz and carrier at 43.7 ppm. Corresponding ^{13}C-^{13}C TOCSY spectra were recorded for the ^{13}C resolved NOESY experiments with mixing times of 27 ms (for a review of these methods, see ref *27*). A ^{13}C-HSQC NOESY-Jump-Return experiment (*20*) was recorded to obtain NOEs from those α protons that were very close to water and could not be obtained from the ^{13}C-NOESY HSQC experiment. Additionally, a ^{13}C resolved NOESY spectrum with ^{13}C spectral width of 24 ppm and carrier at 123 ppm was recorded to assign NOEs arising from aromatic protons. HA, CA, CO and CB chemical shifts were used to obtain dihedral angle and hydrogen bond restraints using the program CSI (*21*).

Intermolecular NOEs were obtained using three isotope-filtered experiments (*22*). Two 3D $^{13}C/^{15}N$ F_1-filtered, F_3-edited NOESY−HSQC (500 ms) and a 2D $^{15}N/^{13}C$ filtered NOESY (400 ms) were recorded to identify intermolecular and intrapeptide NOEs, respectively. As a result, intermolecular NOEs for the peptide backbone as well as side chain protons were obtained. Additionally, a modified HNCO-TROSY experiment (*23*) was recorded to obtain hydrogen bonding atoms in the protein. The experiment was carried out with a protonated protein, accounting for the fact that only 2 of such restraints (34HN-55CO, 89HN-101CO) were obtained.

Structure Determination. Using a combination of 3D ^{15}N (80 ms), ^{13}C (120 ms), $^{15}N^{13}C$ (100 ms), and $^{13}C^{13}C$ (120 ms) resolved ^1H-^1H NOESY spectra, 2941 NOEs were manually and unambiguously assigned using the XEASY graphical interface (*17*). To obtain distance constraints, all of the peaks picked in the 3D singly ^{15}N and ^{13}C resolved NOESY spectra, assigned and otherwise, were integrated at an appropriate threshold using the "peakint" module of the program XEASY (*17*). A list of 3222 integrated NOEs was obtained, from which 2941 were unambiguously assigned and 281 had ambiguous (multiple) assignments. In addition, 76 ϕ and ψ dihedral and 76 hydrogen bonding restraints (2 for each hydrogen bond) derived from the Chemical Shift Index (*21*) were obtained. The topology and parameter files were modified to include phosphotyrosine and acetylated and amidated termini for the peptide, based on the data present at http://xray.bmc.uu.se/hicup/ (*24*).

First, a preliminary protein structure was calculated using the program CNS (Crystallography and NMR System, ref *25*) without the peptide, using the standard simulated annealing (SA) protocol for torsion angle dynamics, based on the 2941 manually assigned distance restraints. The violated restraints in this structure were checked and reas-

[1] Abbreviations: NMR, nuclear magnetic resonance; CPMG, Carr−Purcell−Meiboom−GillR; MSD, root-mean-square displacement; R_1, longitudinal spin relaxation rate; R_2, transverse spin relaxation rate; NOE, nuclear Overhauser effect; CSI, chemical shift index; ARIA, ambiguous restraints in iterative assignment.

Table 1: Input Restraint Summary and Structure Statistics for 25 Lowest-Energy Structures of the YopH Complex

total NOE distance restraints	3222	
unambiguous	3178	
intraresidue	1325	
interresidue	1853	
sequential	717	
medium range	443	
long range	693	
ambiguous (not used in final ensemble)	44	
intermolecular	17	
hydrogen bonds[a]	98	
ϕ	76	
ψ	76	
average geometry, restraint and energy statistics (CNS)		
bond length violations (number)	0	±0
bond angle violations (number)	1.7	±1.1
bond angle RMSD (deg)	0.59	±0.03
improper violations (number)	1.55	±0.94
improper RMSD (deg)	0.49	±0.035
close contacts < 1.6 Å (number)	2.75	±1.83
NOE violations > 0.5 Å (number)	0	
NOE violations 0.2...0.5 Å (number)	6.85	±2.2
NOE RMSD (Å)	0.023	±0.0018
dihedral violations > 5° (number)	0	
dihedral violations 2...5° (number)	3.5	±1.4
dihedral RMSD (deg)	0.61	±0.06
total Energy (kcal)	592	±63
NOE energy (kcal)	114	±17

atomic rms deviations (Å)	backbone	heavy atoms
Protein		
all[b]	0.63	1.01
structured elements[c]	0.45	0.75
Peptide		
all	1.38	1.78
PTR (all atoms)		1.20

[a] Two restraints were included per hydrogen bond to maintain linearity. [b] Residues 5−125. [c] Defined as residues 5−16, 24−27, 31−34, 50−62, 70−80, 88−94, 97−103, 110−124.

signed wherever possible; others were kept for subsequent calculations.

Next, the lowest-energy structure thus calculated was used as the starting structure for an iterative assignment of the remaining 281 ambiguous NOE restraints using the program ARIA 1.0 (Ambiguous Restraints in Iterative Assignment, ref *26*) integrated with CNS (*25*). The following protocol was employed (*26*): 20 structures were generated in each of every nine iterations, out of which seven structures with the lowest total energy were used for the purposes of ensemble-based assignment of ambiguous NOEs (using r^{-6} weighing) and recalibration of distances based on a relaxation matrix integration. Ten lowest-energy structures from each iteration were kept as starting structures for the next iteration, in which an additional 10 were calculated ab initio with a random torsion angle SA protocol. The values of the ambiguous NOE cutoff parameter in the nine iterations were 0.999, 0.999, 0.99, 0.99, 0.98, 0.96, 0.93, 0.90, and 0.80 (the smaller the value of cutoff, the fewer peaks remain unambiguous; ref *26*). After the ninth iteration, the resulting structures showed good convergence, with a backbone RMSD of the secondary structure elements (defined in Table 1) of 0.44 Å from the mean for 10 structures. The restraints classified as ambiguous were checked and assignments were corrected in some cases. The final result was that 44 NOE restraints remained ambiguous; these were discarded in the following calculations.

Next, CNS was used to generate random conformations of the peptide. These were docked onto the 10 protein structures obtained from the final ARIA calculation using a set of 21 intermolecular NOEs and the standard simulated annealing protocol in CNS and using the last set of unambiguous intraprotein distance restraint upper and lower bounds as defined by the final ARIA iteration. Electrostatic interactions were not switched on as to avoid biasing the position of the heavily charged peptide. Since the intermolecular NOEs were obtained from NOESY experiments with long mixing times, these were used only as qualitative, loose restraints. For all the peaks that could be assigned, the lower and upper limits were set at 0 and 6 Å, respectively. For the same reason, no intrapeptide NOEs were used as distance constraints. Two sets of two out of the 21 intermolecular NOEs were violated in many structures. These were between the peptide side chains and the β protons of residues Lys114 and Lys75 of the protein. These were checked and found not to be on the list of residues mapped from chemical shifts changes. Interestingly, these protein residues form a positively charged patch located at the opposite side of the protein as where the peptide binding site is found to be located. This

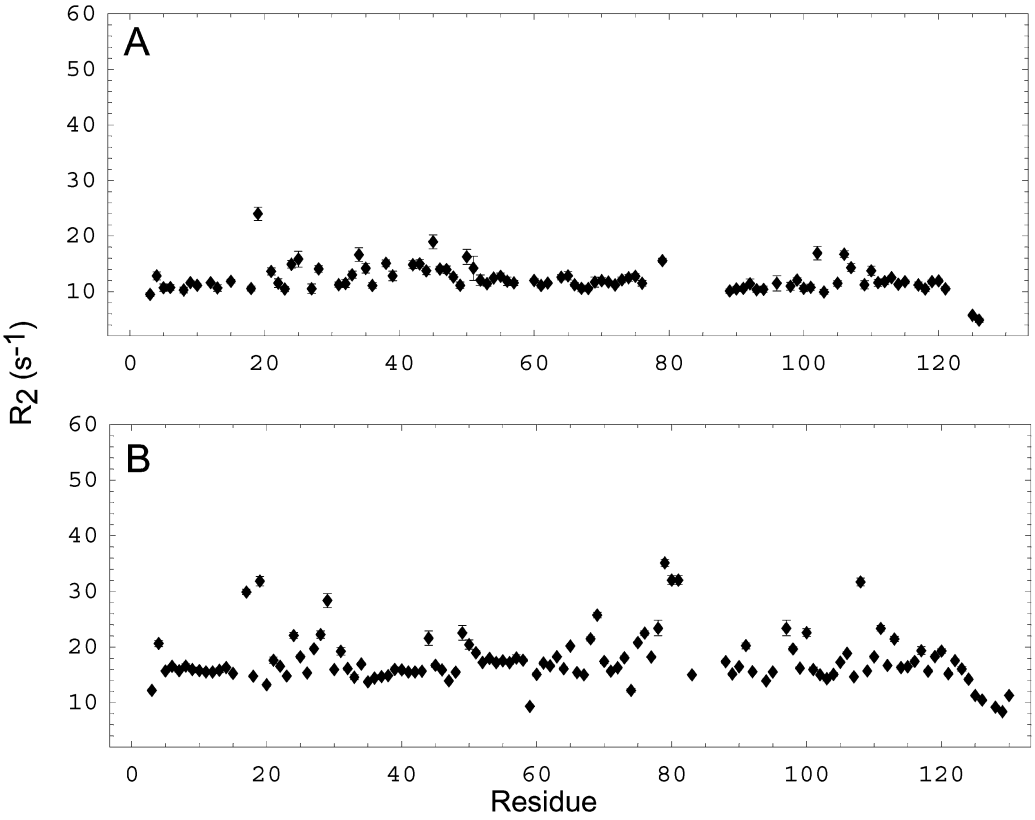

FIGURE 1: ^{15}N R_2 ($1/T_2$) relaxation at 18T in apo-YopH-NT (Panel A) and YopH-NT complexed with Ac-DEpYDDPF-NH_2 in a 1.2:1 molar ratio (peptide:protein) (panel B). The data are plotted as a function of the residue number. Error bars reflect experimental errors in measurement. Missing data points result from residues that did not have assigned resonances. The experiments were recorded without the use of a CPMG sequence so as to not suppress conformational exchange broadening (*32*).

may indicate nonspecific binding and these NOEs were excluded from further calculations.

Finally, the best of the resulting complex structures was further refined with CNS, using a standard torsion dynamics simulated annealing protocol and using the last set of unambiguous intra-protein distance restraint upper and lower bounds as defined by the final ARIA iteration and the 19 remaining intermolecular NOEs. Twenty-eight additional hydrogen bonding restraints between β-sheets 24−27:31−34 and 88−94:97−103 were added to the hydrogen bond list to regularize the geometries of these β-sheets. Forty structures were obtained in the final round of calculation,s of which the 20 with lowest energy and best stereochemistry are discussed here and were submitted to the protein data bank, accession number 1M0V.

RESULTS

Rotational Correlation Time. ^{15}N R_2 relaxation rates were measured for ^{15}N-labeled YopH at 18 T in the presence and absence of Ac-DEpYDDPF-NH_2 (Figure 1). The average T_2 relaxation time ($1/R_2$) for the majority of the residues in the apo-protein was 90 ms. The mean value for the T_1 ($1/R_1$) was 876 ms (results not shown). From these values, we calculated a rotational correlation time of 7.1 ns, which corresponds to a hydrodynamic radius of 1.99 nm, using the Stokes−Einstein relationship (*27*). This number is in excellent agreement with the hydrodynamic radius of 2.1 nm obtained from the dynamic light scattering studies of a purified monomeric form of YopH-NT (*13*) and the theoretical value of 1.94 nm predicted for a 14.8 kDa protein, assuming a single hydration shell and a specific volume of 0.73 cm^3 g^{-1} (*27*). This proves that the YopH-NT apo-protein is a monomer of 14.8 kDa in solution at the conditions used.

The mean T_2 relaxation rate for the majority of the resonances in the peptide-bound protein was 67 ms as shown in Figure 1B. This indicates a 30% increase in apparent hydrodynamic volume upon peptide binding. This is fully explained by our structural data, which show that the bound peptide increases the average protein radius by approximately 10% as it binds to a very shallow cleft on the surface of the protein.

Structure Calculation. On the basis of the above results, the three-dimensional structure of YopH-NT/peptide complex was modeled as a monomer. The final ensemble of 40 structures was calculated with CNS using 3178 unambiguous distance restraints, 44 ambiguous restraints, and 152 dihedral and 98 hydrogen bonding restraints. All the structures converged and exhibited good geometry, with no distance violations >0.5 Å or dihedral violations $>5°$. Superposition of the main-chain atoms for the 25 lowest-energy structures of the complex (Figure 2) had an RMSD of 0.45 Å from the average for the main-chain atoms and 0.75 Å for all heavy atoms in the ordered regions of the protein (see Table 1). The loop regions on the protein, which had fewer NOEs than the rest of the molecule, are seen to have larger RMSDs. Due to the availability of only a limited number of intermolecular NOEs and no intrapeptide NOEs, the N-terminal region of the phosphopeptide backbone is seen to span a large conformational space. Nevertheless, the phosphotyrosine side chain is restricted. The C-terminus of the

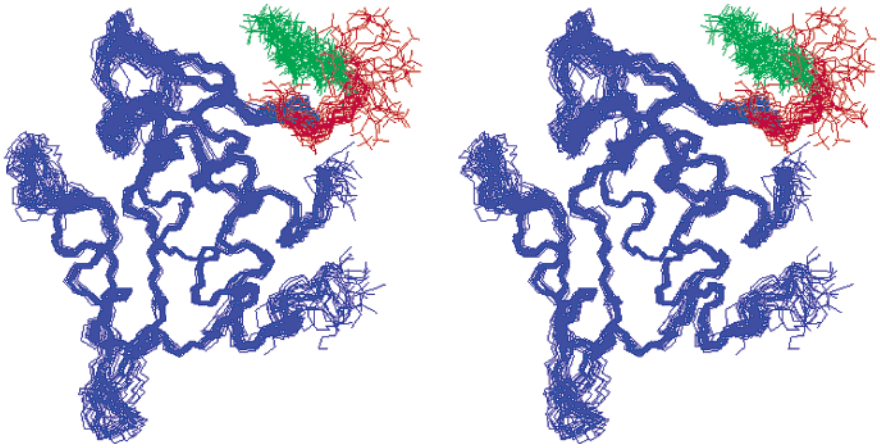

FIGURE 2: Ensemble of the 25 lowest-energy structures of YopH-NT complexed with *N*-Ac-DEpYDDPF-NH_2 superimposed using all backbone atoms of the protein. Protein backbone is in blue, peptide backbone in red, and the Ptr (phosphotyrosine) side chain is shown in green. Twenty members of this ensemble are deposited at the protein data bank, accession code 1M0V.

Table 2: Intermolecular NOEs between YopH-NT and the Peptide Ac-Asp202-Glu 203-Ptr 204-Asp 205-Asp 206-Pro 207-Phe 208-NH_2

Gly 29 HN	Glu 203 HB
Asn 30 HN	Glu 203 HB
Arg 28 HN	Ptr 204 HD
Asn 30 HN	Ptr 204 HE
Ala 32 HN	Ptr 204 HD
Leu 8 HD	Pro 207 HA
Leu 8 HD	Pro 207 HB
Leu 8 HD	Pro 207 HG
Leu 8 HD	Pro 207 HD
Arg 10 HN	Phe 208 HZ
Gln 11 HN	Phe 208 HE
Arg 14 HN	Phe 208 HE
Leu 15 HN	Phe 208 HD
Leu 15 HA	Phe 208 HD
Arg 10 HA	Phe 208 HE
Asp 7 HB1	Phe 208 HD
Asp 7 HB2	Phe 208 HD

peptide is seemingly better defined, since 12 out of 17 NOEs arise from this region (see Table 2). Analysis of the ensemble of the complex structures by PROCHECK (*28*) revealed that, on average, 88.3% and 9.0% of the backbone angles lay in regions of Ramachandran space classified as favorable/allowed or generously allowed, respectively. Of the remaining average 2.6% classified as disallowed, the residues lie in the disordered segments of the protein (2, 39, 44, 66, 87, 105) or on the peptide (Asp202, Glu203). The structure with model number 9 in the PDB ensemble 1M0V has no Ramachandran violations.

Structure of the Complex. A ribbon model of a representative structure is shown in Figure 3. The YopH-NT protein consists of four α-helices (residues 5−18, 51−63, 70−81, and 110−124) and two double-stranded *β*-sheets (24−28: 30−34 and 87−94:96−103) and various loops connecting these secondary structural elements. The locations of these elements correspond closely to the X-ray structures, with the exception of the third helix that is three residues shorter at its C-terminus compared to the X-ray structure. This is caused by a lack of NOEs due to a paucity of resonance intensity in the loop connecting this helix and the second *β*-sheet most likely because of extensive dynamic processes. The highly negatively charged peptide is located in a region on the protein with a net positive electrostatic charge caused by a cluster of basic residues on the surface including Arg 28, Lys 26, and Arg 49 (Figures 3−5). The peptide-binding region of the protein is located near the N-terminus, with the first α helix and *β*-heet contributing many residues (residues 8−15 and 26−34, respectively) to the interface. Some of the residues from the loop close to the second α helix (residues 48 and 49) also interact with the peptide. In our structure calculations and refinements, electrostatic interaction terms were switched off as to not bias the localization of the peptide. Nevertheless, the phosphate group of the tyrosine residue on the peptide interacts very closely with the NH_3^+ group in the side chain of Lys 26 (Figure 5). An analysis of the distances between atoms from the peptide with those on the protein shows that in more than 18 of the 25 conformations, the distance between NZ of Lys 26 and O(P) of phosphotyrosine (Ptr) residue of the peptide is between 2.84 and 4.98 Å and that between HZ1 and O(P) is 1.94−4.79 Å. Moreover, more than 10 structures have short distances between NZ and O3P (2.62−4.84 Å), HZ2 and O3P (2.47−4.98 Å), and HZ1 and O3P (2.22−4.79 Å) suggesting specific electrostatic and hydrogen bonding interactions. This may explain why YopH-NT selectively binds phosphotyrosine-containing peptides. Besides these interactions between the protein side chain atoms and the phosphotyrosine group on the peptide, there are various other charge interactions between Asp 202 and Glu 203 on the peptide and Arg 28 on the protein. For example, NH1 of Arg 28 is close to OE1 of Glu 2 (2.75 to 4.83 Å) in at least eight structures.

Figure 6a shows an overlay of the monomeric crystal structure (*14*) and the average NMR structure. The structures compare well (RMSD of superposition for the backbone atoms of residues 3−125 is 0.80 Å), despite the fact that our structure contains a peptide. The overlay of the dimeric X-ray crystal structure (*13*) and the average NMR structure is shown in Figure 6b. The most salient feature is that peptide binds right at the crossover region of the dimeric structure. Apart from that, the structures are very similar in the monomeric regions: the RMSD of superposition between the two structures for residues 30−125) is 0.87 Å.

Ligand Binding Characteristics. Initially, apo-YopH-NT was titrated with the phosphotyrosine peptide DADEpYL derived from the epidermal growth factor receptor and

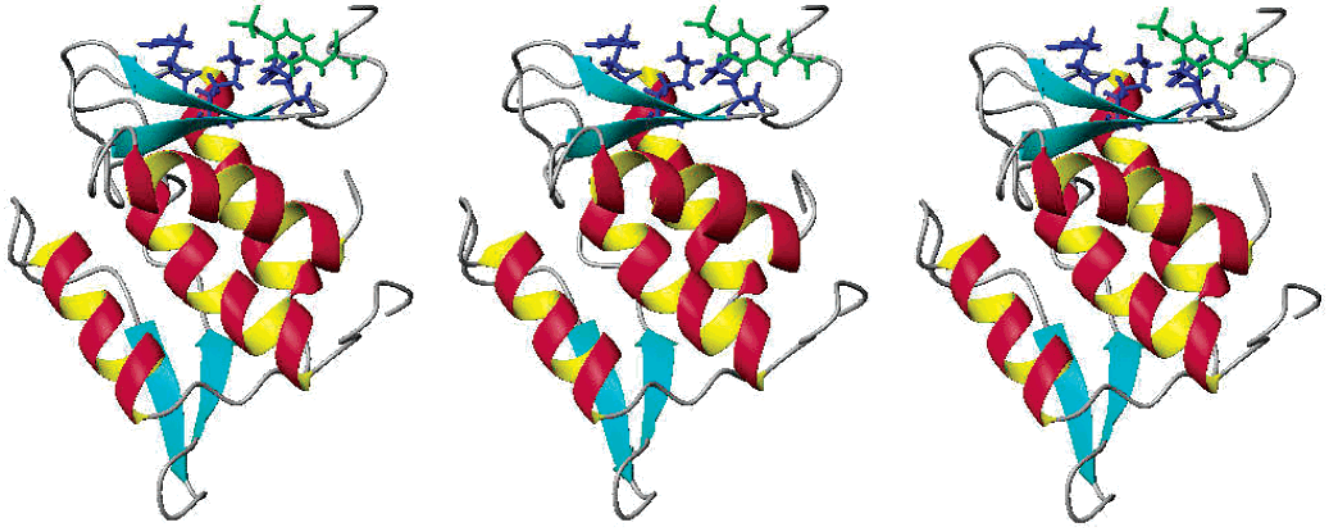

FIGURE 3: Stereo drawing of the average structure of YopH-NT. This figure combines regular (wall-eyed) stereo and cross-eyed stereo for the reader's convenience. The left-eye image is at the center; the right-eye image is displayed twice. The phosphopeptide is at the top right, and the location of the phosphotyrosine side chain is indicated in green. Several positively charged protein side chains in the vicinity of the phosphopeptide, Lys26, Arg28, and Arg49 are displayed in blue. The figure was generated using Molmol (*40*).

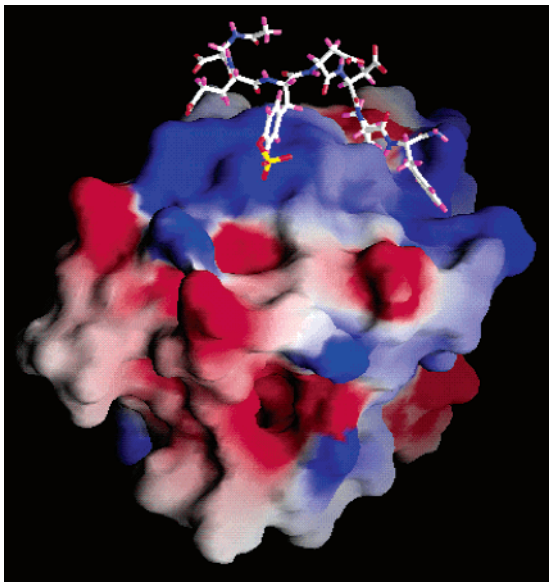

FIGURE 4: Molecular surface of the protein showing negative surface charge in red and positive in blue. The negatively charged peptide binds very close to the large positive patch on the surface. The figure was generated with the software package GRASP (*41*).

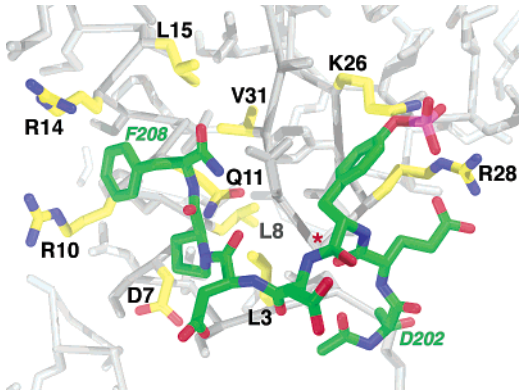

FIGURE 5: One of the lowest-energy conformations of the complex (model 12 of the PDB accession), displaying the peptide binding region. The conformation of the peptide mainchain was regularized using the program "O" (*42*), and the side chain conformations of Lys26 and Arg28 were slightly adapted to optimize contact with the peptide Ptr phosphate group. Labels indicate residues that are discussed in the text; the asterisk indicates Gly29.

previously shown to be a good substrate for the YopH catalytic domain (*29*). The binding process was in the fast exchange regime with little line broadening (Figure 7), and the NMR binding isotherms indicated an equilibrium dissociation constant of approximately 10 micromolar (Figure 8). The ^{15}N shifts were of the order of 1 ppm (80 Hz at 18 T). Kinetic line shape simulations show that these fast exchange data, with minimal linebroadening, are consistent with an off-rate of at least 3×10^3 s^{-1}, leading to an on-rate of at least 3×10^8 M^{-1} s^{-1} (*30*). This calculated on-rate corresponds well to the high-end limit of a diffusion controlled reaction (*31*). These results are relevant to the peptide-binding data with Ac-DEpYDDPF-NH_2 because the DADEpYL peptide affected the chemical shifts of a subset of the residues affected by the Ac-DEpYDDPF-NH_2 peptide (Figure 9). When apo-YopH was titrated with the phosphopeptide Ac-DEpYDDPF-NH_2, the binding process was in the slow/intermediate exchange regime with similar chemical shifts (see Figure 7). Excessive line broadening effects during the intermediate stages of the titration were observed for many of the perturbed protein resonances, which rendered a direct determination from the NMR data of an apparent equilibrium constant for this peptide impossible. However, we still can estimate the affinity in the following manner. Line shape simulations indicate that the observed slow exchange with extensive broadening for shifts of 80 Hz is consistent with off-rates of the order of 30 s^{-1}, i.e., just 100 times slower than that for the DADEpYL peptide. Assuming that the bimolecular diffusion-controlled on-rate is the same as those for the related and similarly charged DADEpYL, we thus estimate an equilibrium dissociation constant that

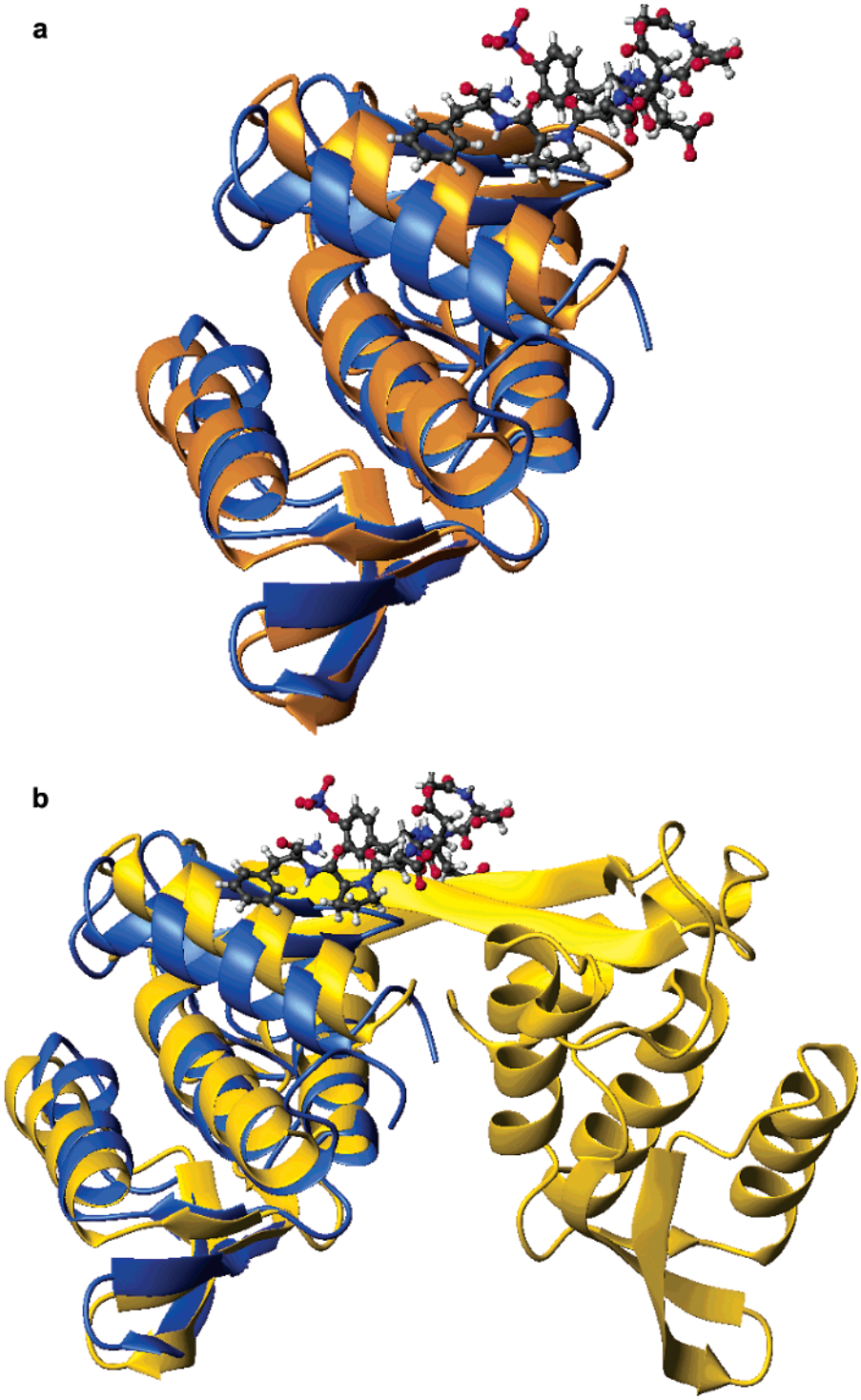

FIGURE 6: Superpositions of the peptide-bound NMR structure (blue) of the complex with the two available crystal structures of apo-protein. Peptide backbone and the phosphotyrosine residue side chain are shown in green. Panel a shows the superposition with the monomeric apo-protein X-ray model in yellow (accession code 1HUF, ref *14*). The RMSD of superposition is for the backbone atoms of residues 3−125 is 0.80 Å. Panel b shows the superposition with one of the apo-protein monomers of the crossover dimer model in yellow as obtained from X-ray diffraction data (accession code 1K46, ref *13*) Note that the peptide binds closely to the crossover junction. Otherwise, the structures are closely related and have a RMSD of 0.87 Å of superposition for residues 30−125. The figures were made with Molmol (*40*).

is 100 times tighter than for DADEpYL, i.e., on the order of 1×10^{-7} M for the Ac-DEpYDDPF-NH_2 peptide.

Conformational Exchange. Figure 1 shows the results of the measurement of the ^{15}N R_2 relaxation rates for YopH-NT with and without the Ac-DEpYDDPF-NH_2 peptide. The experiment was collected with only a single composite 180° ^{15}N pulse in the ^{15}N R_2 period, such that conformational exchange broadening is retained as much as possible (*32*). By examining the ^{15}N R_2 relaxation rate values for individual residues in the apo-protein, we noticed that mainly the residues located between the first two helices (residues 19−50) showed considerably greater line broadening of their ^{15}N resonances (up to 15 s^{-1} excess broadening; see Figure 1A). In addition, resonances for the area 81−85 were missing from

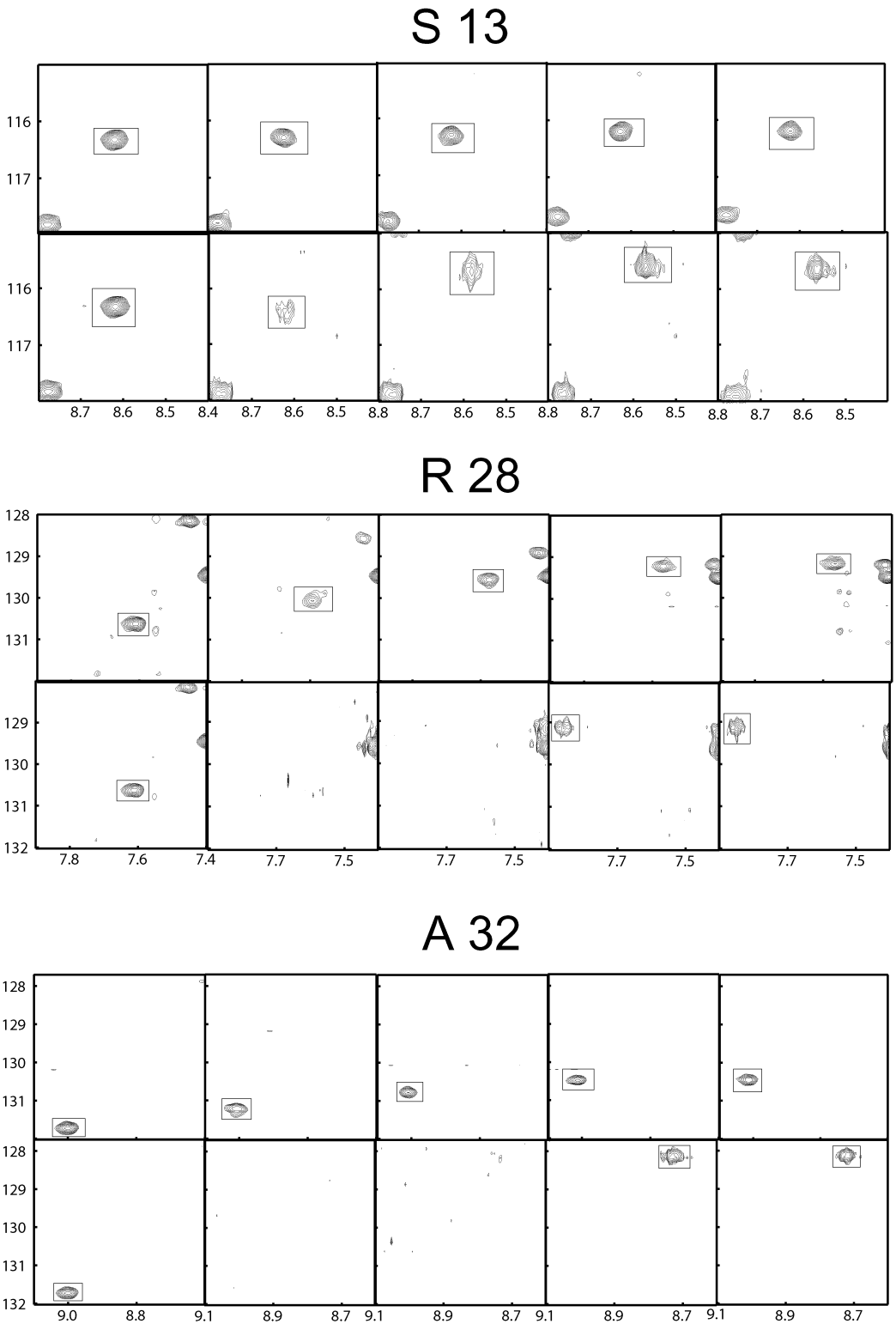

FIGURE 7: Titration of YopH-NT with the phosphotyrosyl containing peptide DADEpYL (derived from epidermal growth factor receptor) (top rows) and Ac-DEpYDDPF-NH_2 (bottom rows). The panels are excerpts from ^1H-^{15}N HSQC spectra of the protein. The peptide/protein molar ratios were, from left to right, 0.0, 0.3, 0.6 1.0, and 1.2. Boxes indicate the cross-peaks of interest. Note that corresponding residues shift in the fast-exchange regime for DADEpYL and in the slow exchange regime for Ac-DEpYDDPF-NH_2. Residue S13 does not shift for DADEpYL.

the NMR spectra. This indicates that these regions in the monomeric protein are undergoing conformational exchange (i.e., adopting different conformations) at the milli- to microsecond time scale. The conformational exchange persists in the peptide-bound form (Figure 1B).

DISCUSSION

Structure Quality. The solution structure of YopH-NT presented here is based on over 3200 direct distance restraints, 2 experimental hydrogen bonding restraints derived

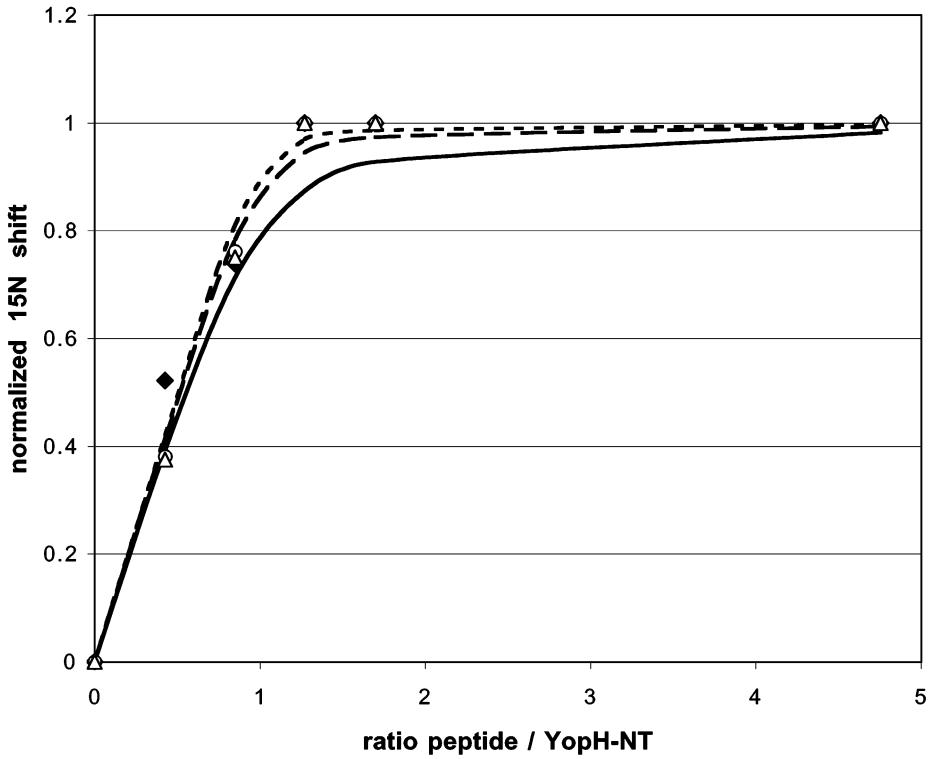

FIGURE 8: Estimation of the dissociation constant for binding of YopH-NT with the phosphopeptide DADEpYL. Data are normalized for fast-exchange shifting ^{15}N resonance positions of residues Val 31 (open triangles), Ala 32 (open circles), and Arg 28 (solid diamonds) obtained from ^{15}N-^{1}H HSQC experiments using an initial protein concentration of 0.6 mM. The theoretical curves in this figure serve to visually bracket the range of dissociation constants compatible with the data. They are calculated from the full quadratic binding isotherm for dissociation constants of 3×10^{-5} (solid), 1×10^{-5} (dashed), and 5×10^{-6} M (dotted).

from a long-range trans-hydrogen-bond HNCO, 98 hydrogen bonds derived from initial structure calculations, and 76 backbone dihedral angle restraints derived from the chemical shift index. The program Aria 1.0 used for the structure calculation contains an relaxation matrix module. This renders the estimation of upper and lower bounds for the constraints from the NMR data unnecessary, while the effects of spin-diffusion are explicitly included. Using the ARIA-calibrated restraint list, this relatively large number of NOEs per residue (25) leads with CNS to an ensemble with an average RMSD from the mean of 0.45 Å on the backbone excluding the loops. We believe that the obtained precision of the backbone structured regions is close to the theoretical limit, as the average root-mean-square fluctuations for similar regions of proteins calculated from molecular dynamics simulations are also in the 0.3−0.5 Å range from the mean structure (see, e.g., ref *32*).

Comparison with X-Ray Crystal Structures. Recently, two groups independently reported X-ray diffraction crystal structures of very similar constructs of the YopH-NT fused to a carboxy-terminal His_6 tag (*13*, *14*). The structures did not include a bound phosphopeptide. Although unit cell, space group, and crystallization conditions were virtually identical in the two structures, one group interpreted the electron density as a compact monomer (*14*), while the other group interpreted the density as a domain-swapped dimer in which residues 1−29 crossover and fold with the other molecule of the dimer (*13*). The major difference between the two crystal structures is at Gly 29, where in the monomeric form the polypeptide forms a reverse turn and a β-hairpin while in the dimeric form the polypeptide continues as a β-strand forming a two-stranded β-sheet with the identical region of the other molecule. Smith et al. (*13*) demonstrated that both monomer and dimer were present in the protein solution used for crystallization (pH 7.5) and that the monomer was most stable at low pH.

The NMR data provides very strong evidence that the YopH-NT structure is monomeric in solution and very similar to the monomeric model put forth by Evodokimov et al. (*14*). First, the correlation time of the protein as measured by ^{15}N relaxation data is 7.1 ns, characteristic of a molecule of 14 kDa at 25 °C (see results). Moreover, ^{15}N-isotope-filtered NOE experiments using a concentrated and well-equilibrated mixture of ^{15}N labeled and unlabeled YopH-NT did not show any intermolecular NOEs (results not shown), consistent with a monomeric structure. Finally, the chemical shift indices, derived from the chemical shifts of four nuclei, show a discontinuity in the β-sheet (*24*−*34*) at residues 28 and 29 (results not shown). Such a discontinuity would be most consistent with the solvent-exposed tight turn present in a monomeric structure, and not with a more rigid intermolecular β-sheet formed by these residues in the domain-swapped dimer.

A rather dramatic difference exists for the position of the first helix in the monomeric X-ray and the NMR structure (see Figure 6a). As we argue below, this difference is unlikely to be caused by the absence/presence of phosphopeptide. Interestingly, the same difference exists for this helix between the NMR structure and the dimeric crystal structure (Figure 6b); indeed, both crystal structures superimpose very well. In this context, we note that Smith et al. (*13*) have argued that both crystal structures actually represent identical crossover dimers because the crystals were in both cases grown at high pH, where a dimeric form is prevalent in

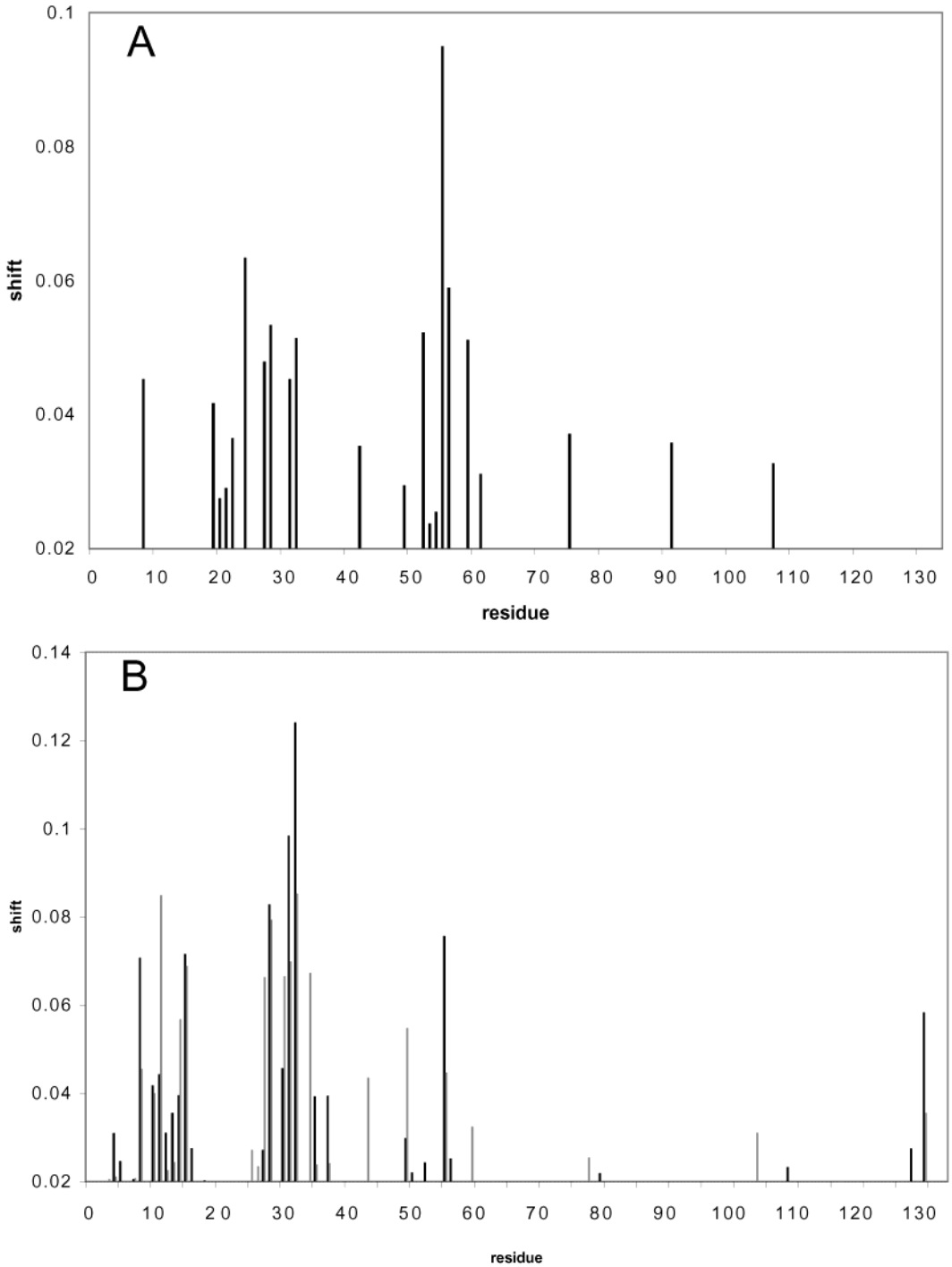

FIGURE 9: Chemical shift perturbation of YopH-NT up on peptide binding. Panel a shows data for the binding of DADEpYL, calculated as shift = $((\Delta^{15}N/25) + (\Delta^{1}HN/3.6))/2)^{1/2}$ obtained from titration shifts in fast exchange. Panel b shows data for the binding of Ac-DEpYDDPF-NH_2, calculated as shift = $((\Delta^{15}N/25) + (\Delta^{1}HN/3.6) + (\Delta^{1}Ha/25) + (\Delta^{13}Ca/3.6) + (\Delta^{13}CB/25) + (\Delta^{13}CO/3.6))/6)^{1/2}$ from the independently assigned chemical shifts of the apo-protein and the complex.

solution. If so, the difference in the position of the first helix in both of the X-ray structures and the NMR structure is due to the difference in dimeric versus monomeric structure. This may be expected because it is precisely this helix that is involved in the domain swap (*13*).

Details of the Complex Interaction. The NMR structure of the YopH protein complex with the phosphopeptide yields insight into the mechanism of peptide binding in a phosphotyrosine-dependent manner. The highly negatively charged peptide binds to a location on the protein that has a high positive charge on the surface, due to the presence of a cluster of positively charged side chains of Arg 10, 14, 28, and 49 and Lys 26 and 35 (Figures 3− 5). The presence of negatively charged side chains on the peptide, such as Asp 202, Glu 203, Ptr 204, Asp205, and Asp 206, provide a favorable charge-based interaction between the peptide and the protein. The position of the peptide is determined with limited precision. This is due to the presence of only a small number of intermolecular NOEs (Table 2), which is not unexpected for a charge−charge interaction. The NOEs are rather widespread on the protein surface (Figure 5). For instance, the peptide Phe 208 residue is in contact with an

extended patch of residues (Table 2), including Asp7 and Leu15, which are on average 11.5 Å apart (see Figure 5). We take the NOE data to indicate that the peptide residue can dynamically visit many locations. Similarly, the phosphotyrosine side chain location is not very well defined, but the ensemble of structures consistently show it to be in the vicinity of the positive side chains of Lys 26 and Arg 28 (see Figure 5). On the other hand, our structural ensemble consistently shows that the side chain of Pro 206 quite precisely covers a hydrophobic patch composed of residues Leu 3 and Leu 8 (see Figure 5). This is evidenced by the presence of a single set of four unambiguous and strong intermolecular NOEs tying the Pro to Leu 8 (see Figure 5). The absence of NOEs between Pro206 and other residues is quite puzzling, especially with respect to Leu3, which according to all low-energy structural models is in its close proximity. Fuller access of the Pro residue to a hydrophobic cleft between residues Leu3 and Leu8 is prevented by the side chain of Gln11, which is very well-defined in the NMR structure (Figure 5). Figure 9 reports the chemical shift mapping of the peptide. Residues affected were 8−11, 14−15, 26−28, 30−32, 34, and 49 and, to a lesser extent, residues 50−55. These residues, except for 50−55, mostly overlap with those identified by the intermolecular NOEs. This underscores that a relatively extended area is perturbed by the peptide. The shifts for residues 50−55 of the second α-helix occur predominantly in the ^{15}N resonance frequencies. Model quantum mechanical calculations indicate that such effects are likely to result from changes in local electrostatic field rather than from conformational change, which would likely also affect the proton chemical shifts (*23*). Therefore, we cautiously interpret the shifts in residues 50−55 as electrostatic, rather than conformational. A possible exception is the shift for residue Phe 55, which lies under the hydrophobic patch covered by the peptide Pro residue. In summary, we conclude that the intermolecular NOEs and chemical shift perturbation identify the same area of interaction. This strongly indicates that there is no long-range conformational (allosteric) change in YopH-NT upon peptide binding. Therefore, the difference of the position of the first helix in the X-ray and the NMR structures unlikely to be caused by the absence/presence of phosphopeptide (see Figure 6a). Otherwise, extended shift changes should be observed in the contact area between this helix and the fourth helix (residues 110−124), which lies directly under it (see Figure 3). Such shifts are not observed (Figure 9).

Our chemical shift mapping studies with the phosphopeptide DADEpYL identified mostly a subset of the interaction surface as mapped by the specific peptide Ac-DEpYDDPF-NH_2 (see Figure 9). The extent of the chemical shifts caused by the phospho-tyrosyl group is similar, but indicative of different off-rate kinetics and affinity (see Results). This includes the long-range electrostatic effects of the shifts in the 50−55 region. Most of the chemical shift changes for residues 8−15, which are in the vicinity of the Pro and Phe residues in Ac-DEpYDDPF-NH_2, are missing for DADEpYL, with the unexplained exception of L5. The combined data suggests that the Ptr group of both peptides bind similarly, such that the additional binding free energy of Ac-DEpYDDPF-NH_2can be attributed to the hydrophobic interactions of the Pro and Phe residues with the protein. This latter interaction thus accounts for the change in dissociation constant from 10^{-5} to 10^{-7} M corresponding to 30% of the overall binding energy of the bound Ac-DEpYDDPF-NH_2 sequence.

Mutagenesis studies have identified four residues (Gln 11, Val 31, Ala 33, and Asn 34) in the amino-terminal domain of YopH that are important for binding to phosphorylated $p130^{cas}$, an in vivo substrate of YopH that contains many YXXP motifs (*34*). Gln11 is directly involved in the binding of the SKAP-HOM-derived peptide binding according to the observed intermolecular NOEs and our derived structural data, and Val 31 is directly adjacent (see Figure 5). The other two residues do roughly map to the same region of the protein as the binding site for the SKAP-HOM-derived peptide DEpYDDPF, but are a little further removed.

Comparison with SH2. The interaction of Ac-DEpYDDPF-NH_2 with YopH-NT is somewhat reminiscent of the interaction of the phospholipase C-γ1 SH2 domain with the phosphopeptide DNDpYIIPLPDPK (*35*). Here, too, the Pro residue is bound in a hydrophobic area, and Ptr is in a positively charged area (see Figure 10). Besides this, there is no similarity between this SH2 domain and YopH-NT. At the level of the protein, there is no homology between any of the SH2 domains and YopH-NT (*13*); the former are predominantly β-sheet proteins, the latter is predominantly α-helical. While the peptide in the SH2 domain is completely extended, the peptide in some of the YopH-NT ensemble structures are strongly curved over residue Gly29, which forms a tight turn between β-strands 1 and 2. Notwithstanding these structural differences at the peptide backbone level, the differences between the essential recognition groups Ptr and Pro in the two structures is not that large: 10 Å in SH2 and 9−12 Å in the YopH ensemble. Therefore, it is quite likely that both proteins can bind to the same targets.

Peptide Binding Mode and the Domain-Swap Dimer Crystal Structure. Recently, the HIV-inactivating protein cyanovirin-N was also found by NMR to be a monomer in solution and a domain-swapped dimer by X-ray crystallography (*36*). Apparently, such rather spectular differences between solution and crystal occur more often. The authors demonstrated that, in solution, cyanovirin-N can exist both in monomeric and in domain-swapped dimeric form, the latter a metastable form (*36*). Also, for YopH, it is implied, since it can exist as a crossover dimer in the crystal, that it can also exist in that form in solution. Indeed, light-scattering data suggest the existence of a substantial fraction of dimeric species at higher pH (*13*); whether this is a crossover form or not is for YopH not known. At neutral and low pH the dimer form is metastable. The crossover dimer in YopH is more than an interesting phenomenon of protein thermodynamics. As shown in Figures 3 and 5, the peptide Ac-DEpYDDPF-NH_2 binds exactly at the locus of the dimer interface over the N-terminal helix and the reverse turn centered at Gly 29. The Pro residue, which is part of the conserved Crk SH2 domain motif pYxxP, makes hydrophobic contacts with residues at the interface between the helix and β-strand 30−34. In the domain-swapped dimer observed in one of the crystal structures (*13*), the reverse turn at Gly29 is not present because it is at this point where the polypeptide changes direction to crossover to the other monomer. Consequently, the peptide cannot bind in an identical fashion in the dimer. Unexpectedly, however, recent calorimetric studies show that Ac-DEpYDDPF-NH_2 binds to purified

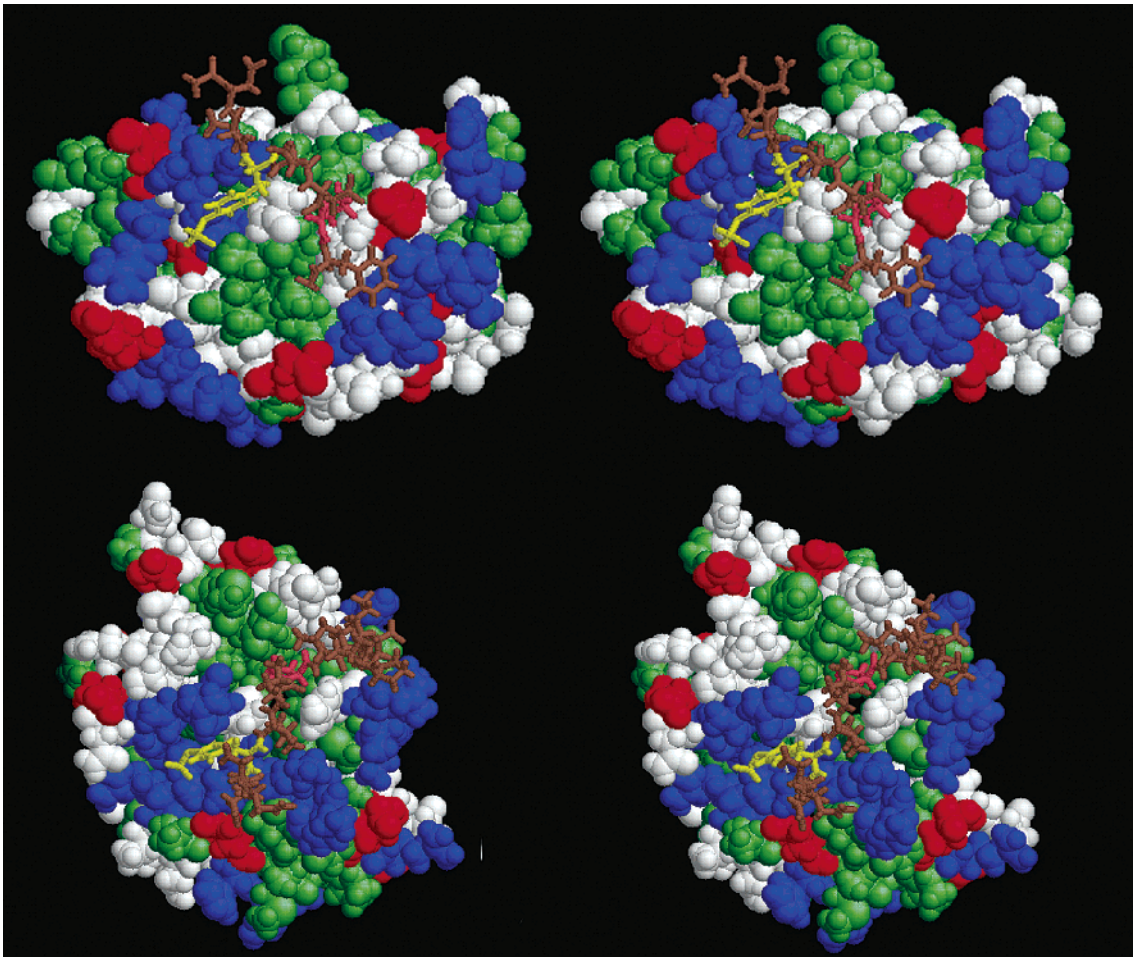

FIGURE 10: Comparison of the current structure of the YoPH-NT/Ac-DEpYDDPF-NH_2 complex with the phospholipase c-γ-1 SH2 domain complexed with DNDpYIIPLPDPK (PDB code 2PLE; ref *35*). The peptide sequence pYXXP is colored brown, with the Ptr in yellow and the Pro in red in both structures. The protein coloring is as follows: green, hydrophobic; red, acidic; blue, basic; white, polar.

dimeric YopH-NT about 40 times tighter than it does to purified monomeric YopH-NT (M. A. S. and J. Vijayulakshmi, unpublished data). Potentially, the dimer provides additional Arg and Lys residues coming from the second molecule that can ligate to the peptide carboxylate side chains of Asp 202 and Glu 203, which in the monomeric structure are completely solvent-exposed. Consequently, even though the full YopH protein, including the phosphatase domain, is monomeric in vitro (*37*), it cannot be excluded that dimeric forms could function as well.

Conformational Exchange. The ^{15}N R_2 relaxation rates for individual residues in the apo-protein showed considerably greater line broadening of their ^{15}N resonances (up to 15 s^{-1} excess broadening than the average; see Figure 1A). This indicates that these regions in the monomeric protein are undergoing conformational exchange (i.e., adopting different conformations) at the milli- to microsecond time scale (for a recent review, see ref *38*). Most of the conformational exchange is observed at the peptide-binding site, which includes the polypeptide involved in the crossover in the dimer crystal structure. The conformational exchange broadening persists in the peptide-bound form; indeed, it is enhanced (Figure 1B). This could be caused by slow-exchange lifetime broadening of the protein resonances due to the dissociation of ligand itself. However, using our estimation for the dissociation constant of 10^{-7} M and an 1.2:1 excess of peptide, a full 99% of the protein is ligated at the concentrations used, and line shape simulations show that lifetime broadening is quenched at these conditions (the reassociation process becomes so fast that no phase loss occurs). Nevertheless, given the uncertainties in the rate and dissociation constant determinations, lifetime broadening cannot be excluded. Alternatively, it should be considered that the dynamics occurs at the crossover junction, which may indicate a predisposition of this area in the monomeric form to undergo the major conformational rearrangement observed in the crossover dimer. The enhancement of the dynamics would then indicate that the monomeric form is destabilized by the peptide binding enhancing the tendency for YopH-NT to partially unfold (*13*). Finally, one should consider the possibility that the ligand binding characteristics have evolved as to not perturb the dynamics. Similar observations have been made for the SH2 domains, where the dynamics of the methyl side chains of the hydrophobic binding pocket are not perturbed by phosphopeptide binding. However, the time scale of the dynamics measurement was in the pico/nanosecond regime rather than in the milli/microsecond regime (*39*). For SH2 it was argued that such a retention of dynamics would allow for a greater free energy of binding with limited structural complementarity (relatively small enthalpy of binding but no loss of entropy); i.e., it would allow for promiscuous, rather unselective, high-affinity binding. Perhaps similar processes are relevant to YopH as well.

ACKNOWLEDGMENT

We thank Dr. J. B. Bliska (SUNY, Stony Brook) for inspiring this project, Dr. K. John Smith for collecting the anti-filtered NOE data, and Drs. Yuxi Pang and Shawn Y. Stevens for stimulating discussions. Special thanks to Dr. J. Vijayalakshmi for sharing her peptide binding calorimetry data.

REFERENCES

1. Cornelis, G. R., and Wolf-Watz, H. (1997) *Mol. Microbiol. 23*, 861−867.
2. Black, D. S., Marie-Cardine, A., Schraven, B., and Bliska, J. B. (2000) *Cell. Microbiol. 2*, 401−414.
3. Guan, K. L., and Dixon, J. E. (1990) *Science 249*, 553−556.
4. Fauman, E. B., and Saper, M. A. (1996) *Trends Biochem. Sci. 21*, 413−417.
5. Bliska, J. B., Clemens, J. C., Dixon, J. E., and Falkow, S. (1992) *J. Exp. Med. 176*, 1625−1630.
6. Andersson, K., Carballeira, N., Magnussun, K. E., Persson, C., Stendahl, O., Wolf-Watz, H., and Fallman, M. (1996) *Mol. Microbiol. 20*, 1057−1069.
7. Woestyn, S., Sory, M. P., Boland, A., Lequenne, O., and Cornelis, G. R. (1996) *Mol. Microbiol. 20*, 1261−1271.
8. Black, D. S., Montagna, L. G., Zitsmann, S., and Bliska, J. B. (1998) *Mol. Microbiol. 29*, 1263−1274.
9. Black, D. S., and Bliska, J. B. (1997) *EMBO J. 16*, 2730−2744.
10. Marie-Cardine, A., Verhagen, A. M., Eckerskorn, C., and Schraven, B. (1998) *FEBS Lett. 435*, 55−60.
11. Birge, R. B., Fajardo, J. E., Reichman, C., Shoelson, S. E., Songyang, Z., Cantley, L. C., and Hanafusa, H. (1993) *Mol. Cell. Biol. 13*, 4648−4656.
12. Sakai, R., Iwamatsu, A., Hirano, N., Ogawa, S., Tanaka, T., Mono, H., et al. (1994) *EMBO J. 13*, 3748−3756.
13. Smith, C. L., Khandelwal, P., Keliikuli, K., Zuiderweg, E. R. P., and Saper, M. A. (2001) *Mol. Microbiol. 42*, 967−979.
14. Evdokimov. A. G., Tropea, J. E., Routzahn, K. M., Copeland, T. D., and Waugh, D. S. (2001) *Acta Crystallogr., Sect. D: Biol. Crystallogr. 57*, 793−799.
15. Neri, D., Szyperski, T., Otting, G., Senn, H., and Wüthrich, K. (1989) *Biochemistry 28*, 7510−7516.
16. Delaglio, F., Grzesiek, S., Vuister, G. W., Zhu, G., Pfeifer, J., and Bax, A. (1995) *J. Biomol. NMR 6*, 277−293.
17. Bartels, C., Xia, T., Billeter, M., Guntert, P., and Wuthrich, K. (1995) *J. Biol. NMR 6*, 1−10.
18. Johnson, B. A., and Blevins, R. A. (1994) *J. Biomol. NMR 4*, 603−614.
19. Khandelwal, P., Keliikuli, K., Smith, C. L., Saper, M. A., and Zuiderweg, E. R. P. (2001) *J. Biomol. NMR 21*, 69−70.
20. Majumdar, A., and Zuiderweg, E. R. P. (1993). *J. Magn. Reson., B 102*, 242−244.
21. Wishart, D. S., and Sykes, B. D. (1994) *J. Biomol. NMR 4*, 171−180.
22. Zwahlen, C., Legault, P., Vincent, S. J. F., Greenblatt, J., Konrat, R., and Kay, L. E. (1997) *J. Am. Chem. Soc. 119*, 6711−6721.
23. Grzesiek, S., Cordier, F., and Dingley, A. J. (2001) *Methods Enzymol. 338*, 111−133.
24. Kleywegt, G. J., and Jones, T. A. (1998) *Acta Crystallogr., Sect. D 54*, 1119−1131.
25. Brunger, A. T., Adams, P. D., Clore, G. M., DeLano, W. L., Gros, P., Grosse-Kunstleve, R. W., Jiang, J.-S., Kuszewski, J., Nilges, M., Pannu, N. S., Read, R. J., Rice, L. M., Simonson, T., and Warren, G. L. (1998) *Acta Crystallogr., Sect. D 54*, 905−921.
26. Nilges, M., and O'Donoghue, S. I. (1998) *Prog. NMR Spectrosc. 32*, 107−139.
27. Cavanaugh, J., Fairbrother, W. J., Palmer, A. G., III., and Skelton, N. J. (1996) *Protein NMR Spectroscopy*, Academic Press, New York.
28. Laskowski, R. A., MacArthur, M. W., Moss, D. S., and Thornton, J. M. (1993). *J. Appl. Crystallogr. 26*, 283−291.
29. Zhang, Z.-Y., Maclean, D., McNamara, D. J., Sawyer, T. K., and Dixon, J. E. (1994) *Biochemistry 33*, 2285−2290.
30. Carrington, A., and McLachlan, A. (1967) *Introduction to Magnetic Resonance with Applications to Chemistry and Chemical Physics*, Harper & Row, New York.
31. Nakatani, H., and Dunford, H. B. (1979) *J. Phys. Chem. 83*, 2662−2665.
32. Pang, A., Buck, M., and Zuiderweg, E. R. P. (2002) *Biochemistry 41*, 2655−2666.
33. Wang, L., Pang, Y., Holder, T., Brender, J. R., Kurochkin, A., and Zuiderweg, E. R. P. (2001) *Proc. Natl. Acad. Sci. U.S.A. 98*, 7684−7689.
34. Montagna, L. G., Ivanov, M. I., and Bliska, J. B. (2001) *J. Biol. Chem. 276*, 5005−5011.
35. Pascal, S. M., Singer, A. U., Gish, G., Yamazaki, T., Shoelson, S. E., Pawson, T., Kay, L. E., and Forman-Kay, J. D. (1994) *Cell 77*, 461−472.
36. Barrientos, L. G., Louis, J. M., Botos, I., Mori, T., Han, Z. Z., O'Keefe, B. R., Boyd, M. R., and Gronenborn, A. M. (2002) *Structure 10*, 673−686.
37. Zhang, Z. Y., Clemens, J. C., Schubert, H. L., Stuckey, J. A., Fischer, M. W. F., Hume, D. M., et al. (1992) *J. Biol. Chem. 267*, 23759−23766.
38. Palmer, A. G., III., Kroenke, C. D., and Loria, J. P. (2001) *Methods Enzymol. 339*, 204−238.
39. Kay, L. E., Muhandiram, D. R., Wolf, G., Shoelson, S. E., and Forman-Kay, J. D. (1998) *Nat. Struct. Biol. 5*, 156−163.
40. Koradi, R., Billeter, M., and Wüthrich, K. (1996) *J. Mol. Graph. 14*, 51−55.
41. Nicholls, A., Sharp, K., and Honig, B. (1991) *Proteins 11*, 281−296.
42. Harris, M., and Jones, T. A (2001) *Acta Crystallogr., Sect. D 57*, 1201−1203.

BI026333L